EXIT ORDER SEQUENCE BURR PREDICTION ALGORITHM BASED ON RECTANGULAR COORDINATES

Miguel C. Ávila and David A. Dornfeld

mcavila@me.berkeley.edu
dornfeld@me.berkeley.edu

Laboratory for Manufacturing Automation
Department of Mechanical Engineering
University of California, Berkeley

KEYWORDS

Burr formation, exit order sequence, face milling.

ABSTRACT

The derivation and implementation of an algorithm that calculates exit order sequence (EOS) as a planar milling burr prediction tool is presented. EOS expresses the orientation of a cutter relative to the workpiece in terms of the exit order of three points describing the major and minor cutting edges. EOS calculations along the contours of a CAD model are based upon an instantaneous, Cartesian frame of reference centered on the tool spindle axis and oriented in the feed direction. The scheme provides accurate and robust EOS calculations and introduces a "worst-case" approach to select a unique EOS from overlapping tool exit conditions.

INTRODUCTION

Mechanistic models developed for the prediction of machining burrs have been successfully applied in the analysis of orthogonal cutting, oblique cutting, and drilling (Gillespie, 1976; Park, 1995; Ko and Dornfeld, 1996; Park and Dornfeld, 2000; Min et al., 2001). Yet, in face milling, material flow is a high degree of freedom phenomenon that involves multiple cutting edges, rendering mechanistic burr formation analysis unwieldy. In order to expedite the analysis, a kinematic model known as exit order sequence (EOS) was formulated by Hashimura, Hassamontr, and Dornfeld (1995, 1999). The underlying principle of EOS is that, during a cutting operation, the orientation of the cutting edges upon disengagement from the work material influences burr formation. In this context, thanks to the orientation of the cutter, burrs may form preferentially on either the edges of the planarized surface and remain attached to the workpiece, or on edges of the transition material and be removed as this material is cut away. EOS simulations on CAD models of the workpieces enable the selection of tool geometries and tool paths that minimize burr-prone EOS conditions. Adjustment of these kinematical parameters can yield significant reductions in burr size even when tool wear promotes stronger burr formation, since kinematic parameters, under most finishing conditions, are predominant in burr formation. The burr prediction capability of EOS has been experimentally validated in previous investigations using different materials and

cutting conditions (e.g. Hashimura et al. 1999; Ávila, 2004; Shefelbine, 2004). However, in production environments, limitations in predicting burr formation were observed due to the absence of accurate simulation tools. Using the EOS ideal geometric relations introduced by Hashimura et al., an EOS algorithm was developed by Bansal (2002). Notwithstanding, attempts for implementing this algorithm in industrial environments have seen disappointing results insofar as the accuracy of the EOS computations along the edges of an input CAD file.

The objective of this work is to introduce a new EOS algorithm based on a rectangular frame of reference, implemented in C++, and to demonstrate its use along the contours of components in automotive production. The scheme accurately simulates the exit order sequence of a cutter along the edges of a CAD model and robustness is guaranteed by avoiding divergence of floating-point number calculations. Additionally, the algorithm uses a "worst-case" approach for dealing with overlapping EOS conditions.

EOS THEORY

The EOS burr prediction theory ranks burr size according to the exit order of points describing the cutting edges and bases itself on the idealized workpiece-tool interaction model shown in Figure 1 (Hashimura et al., 1995, 1999). The model considers a fly cutting operation with two cutting edges and assumes: (i) rigid tool and workpiece, and (ii) negligible tool nose radius. Three characterizing points of the tool-workpiece interface are defined: the tool tip B, defined by the intersection between the major and minor cutting edges, and points A and C, defined by the uncut chip thickness (*w)* and depth of cut (*d)*, respectively, as shown in Figure 1. Tool geometry is described by axial rake *(α)*, radial rake *(β)*, and lead *(γ)* angles. The exit time of points A, B, and C: t_a, t_b, and t_c, respectively, are given by the expressions (Hashimura et al., 1995):

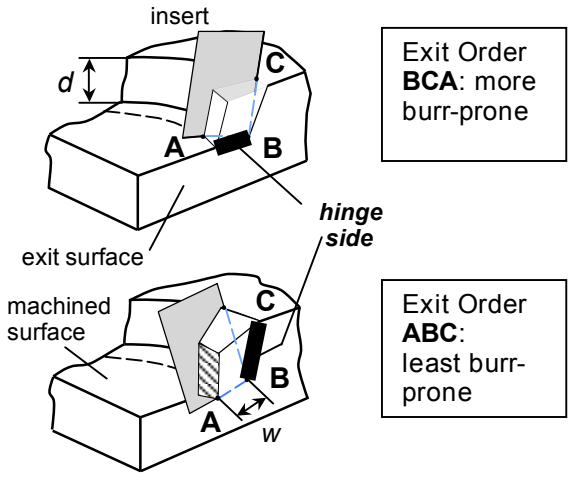

FIGURE 1. EOS MODEL.

$$t_A = \frac{1}{\omega}\{\cos^{-1}(\frac{L}{R_A}) + \sin^{-1}(\frac{\omega}{R_A}\tan\beta)\} \quad (1)$$

$$t_B = \frac{\phi}{\omega} = \frac{1}{\omega}\cos^{-1}(\frac{L}{R_B}) \quad (2)$$

$$t_C = \frac{1}{\omega}\{\cos^{-1}(\frac{L}{R_C}) + \tan^{-1}(\frac{d\tan\alpha}{R_B + d\cot\gamma})\} \quad (3)$$

where R_A, R_B, *and* R_C denote the distances between the spindle axis and points A, B, and C, respectively; L the offset between the tool spindle axis and workpiece; and ω the spindle speed. The model assumes a circular tool locus.

ALGORITHM

Nomenclature and definitions

Figure 2 schematically depicts tool path, cutter locus, feed direction, workpiece edge, and frame of reference at a given instant, viewed from the top in the direction of the spindle axis. The edge partition of the workpiece is defined by points P_1 and P_2, and the material is assumed to be on the right hand side of the contour when the observer moves from P_1 towards P_2. Point P_2 represents the intersection of the instantaneous tool tip locus, P_2 = B, approximated as a circumference of radius $R_B = r$, and the work contour P_1P_2. The Cartesian frame of reference is centered upon the spindle axis, point O, while the xy plane coincides with the machined surface. The x axis is tangent to the toolpath and pointed in the feed direction. Although the algorithm was developed for both forward and reverse tool rotation, for brevity, formulations are given for forward tool rotation only.

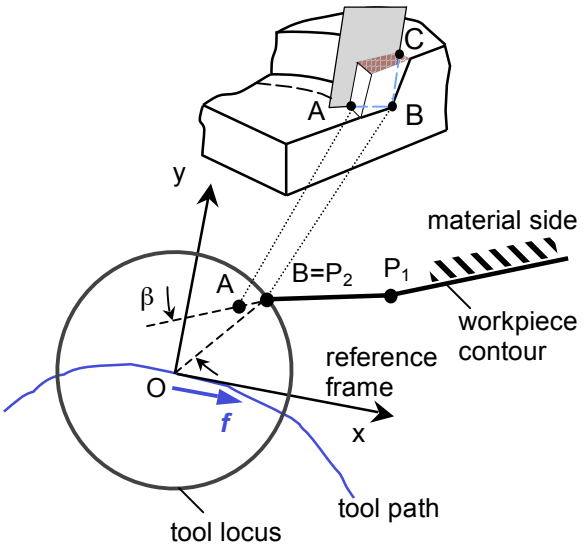

FIGURE 2. SCHEMATIC OF REFERENCE FRAME, TOOL LOCUS, TOOL PATH, CUTTING EDGES, AND CONTOUR OF THE WORKPIECE.

EOS algorithm

Initially, the tessellated contour of the CAD model is separated into tool entrance edges and tool exit edges using the entry/exit algorithm developed by Narayanaswami and Dornfeld (1997) and furthered by Chu (2000). Next, EOS is computed along the tool exit regions to estimate the degree of burr formation on these contours. Tool entrance contours, which are associated with minimized burr formation, undergo no further processing. A flow chart of the algorithm is shown in Figure 3.

In order to calculate the x,y coordinates of A, B, and C, the following inputs are necessary: radius of the cutter ($R_B = r$); axial rake (α), radial rake (β), and lead (γ) angles; depth of cut (d); and feed per tooth (f). A priori, the uncut chip thickness (w) is determined from the relation:

$$w = f\cos\theta \tag{4}$$

where θ is the angular position of the tool tip B with respect to the frame of reference (Figure 4). This angle is computed from:

$$\theta = \tan^{-1}\left(\frac{P_{2y}}{P_{2x}}\right) \tag{5}$$

where (P_{2x}, P_{2y}) are the coordinates of point P_2. Then, it is possible to calculate the x,y coordinates of A, B, and C and define the position of the minor and major cutting edges:

$$A_x = r\cos\theta - w\cos\theta - w\sin\theta\tan\beta \tag{6}$$

$$A_y = r\sin\theta - w\sin\theta + w\cos\theta\tan\beta \tag{7}$$

$$B_x = r\cos\theta \tag{8}$$

$$B_y = r\sin\theta \tag{9}$$

$$C_x = r\cos\theta - d\sin\theta\tan\alpha + d\frac{\cos\theta}{\tan\gamma} \tag{10}$$

$$C_y = r\sin\theta + d\cos\theta\tan\alpha + d\frac{\sin\theta}{\tan\gamma} \tag{11}$$

Once the x,y coordinates are known, it is possible to determine the exit orders of A and C by comparing their positions with respect to B,

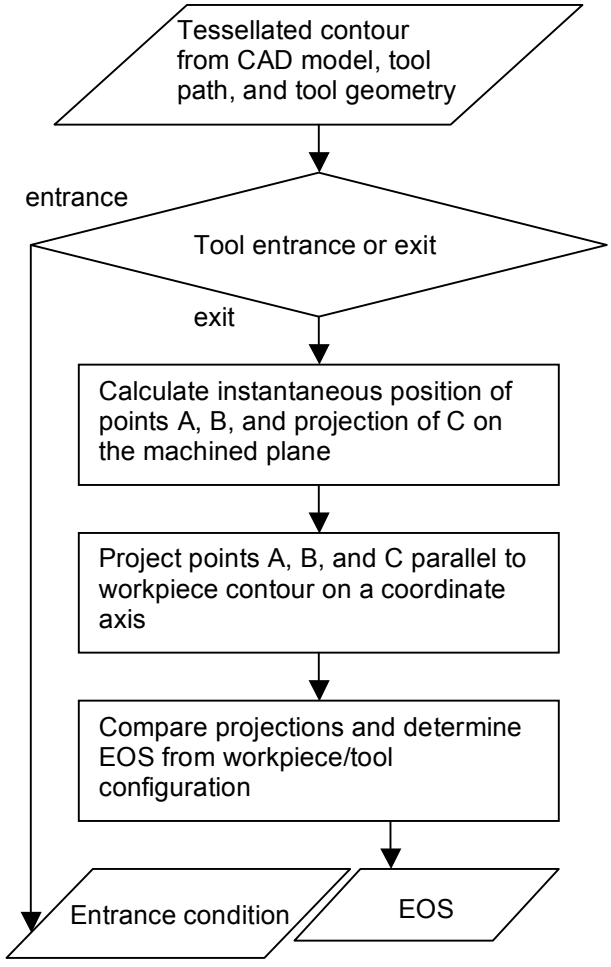

FIGURE 3. EOS ALGORITHM FLOWCHART.

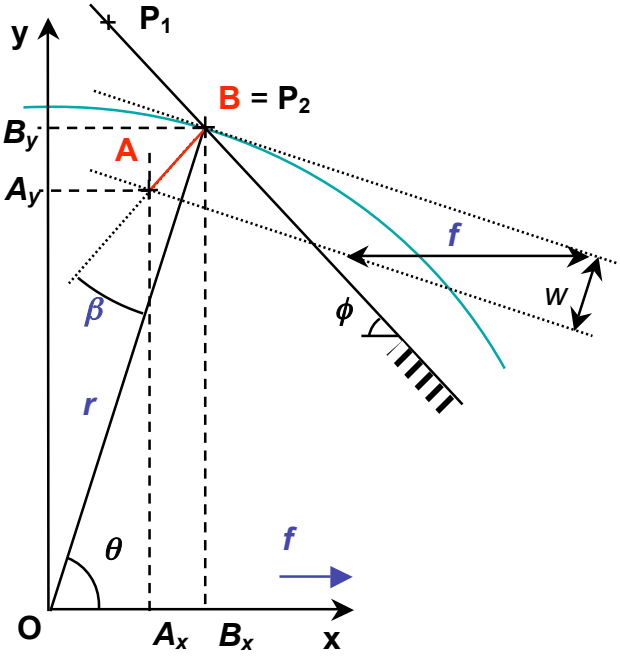

FIGURE 4. COORDINATES OF POINT A GIVEN BY ANGULAR POSITION OF CUTTER TIP *(θ)*, CUTTER RADIUS *(r)*, UNCUT CHIP THICKNESS *(w)* AND RADIAL RAKE ANGLE *(β)*.

which coincides, by definition, with the edge of the workpiece. The methodology is explained as follows. First, the projections of A, B, and C are calculated on the x and y axes, in the direction of the segment P_1P_2. The projections on the y axis, labeled *A'*, *B'*, and *C'* (Figure 5) are given by:

$$A' = A_y + A_x \tan\phi \qquad (12)$$

$$B' = B_y + B_x \tan\phi$$

$$C' = C_y + C_x \tan\phi$$

where $\tan\phi$ is the slope of the workpiece edge contour:

$$\phi = \tan^{-1}\left(\frac{P_{1y} - P_{2y}}{P_{1x} - P_{2x}}\right) \qquad (13)$$

The projections on the x axis are determined, analogously, by simply swapping the y and x components in Equation 12.

Selection between y- and x-projections is devised to prevent divergence of *A'*, *B'*, and *C'*. This selection is triggered by a threshold value of ϕ set a priori. Using y-projections, and assuming the configuration shown in Figure 5, the exit order of A and B is given by the following statement:

IF $\phi < 0$ (slope of contour negative) &&
$P_{1y} - P_{2y} > 0$ (material on the right) &&
$B' > A'$ (proj. of B greater than proj. of A)

THEN B exits before A (14)

The orientation of the material is given by the logical statement:

IF $P_{1y} - P_{2y} > 0$

THEN Material on the left-hand side
ELSE Material on the right-hand side (15)

The conditional statement is chosen according to the orientation of the material with respect to the coordinate system (i.e. whether the material is on the right or left side of segment P_1P_2), and the sign of the slope of P_1P_2. There are 4 possible configurations of material orientations and slope signs, each of which requires a specific IF statement to determine the appropriate exit order. The 4 arrangements are shown in Figure 6, where point C is left out for simplicity. The figure also indicates how the difference between projections *A'* and *B'* is interpreted as an exit order. For illustration purposes, the leftmost arrangement is described

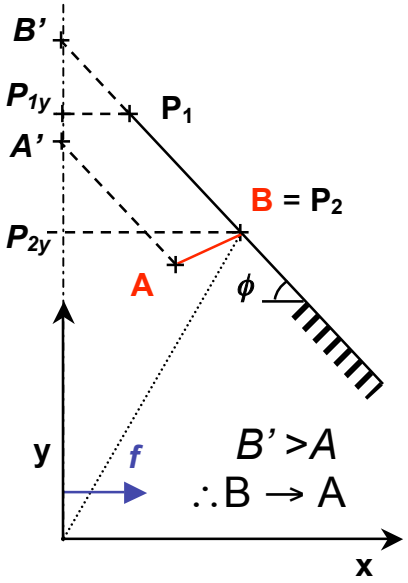

FIGURE 5. PROJECTION OF POINTS A AND B ON THE y AXIS IN THE DIRECTION OF THE CONTOUR.

as follows. If the material lies on the left-hand side of the P_1P_2 segment and $\tan\phi < 0$, the largest projection corresponds to the point which exits the workpiece *first*.

Table 1 presents the logical statements that correspond to each of the six exit order sequences under forward tool rotation. These statements are valid for both y- and x-projection modes.

Worst-case approach

Under EOS theory, exit orders from least burr-prone to most burr-prone are ranked as follows: ABC, ACB, BAC, BCA, CAB, and CBA (Hashimura and Dornfeld, 1999). With certain cutting conditions and tool geometries, however, an overlap of two or more exit order sequences may occur in some regions of the workpiece. An overlap condition is seen when at least 2 projections among *A'*, *B'*, and *C'*, are coincident.

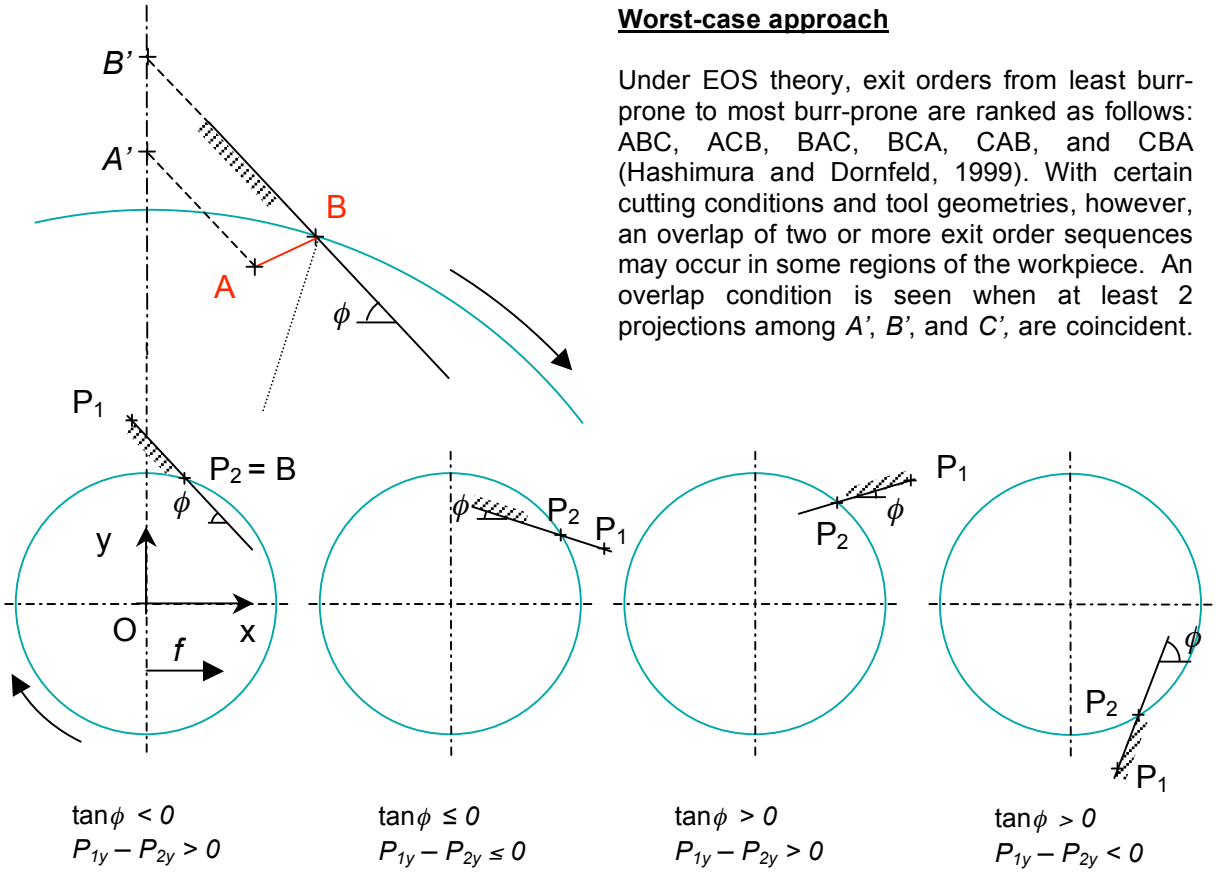

y proj.	Largest exits *first*	Largest exits *last*	Largest exits *last*	Largest exits *first*
x proj.	Largest exits *first*	Largest exits *last*	Largest exits *first*	Largest exits *last*

FIGURE 6. EXIT ORDER DEPENDING ON TOOL-MATERIAL EDGE CONFIGURATION AND RELATIVE VALUES OF THE POINT PROJECTIONS OVER THE AXES.

TABLE 1. LOGICAL STATEMENTS CORRESPONDING TO EACH EOS CONDITION.

Largest projection exits *first*	
EOS	Logical statement
ABC	$C' < B'$ && $B' < A$
ACB	$B' \le C'$ && $C' < A$
BAC	$C' < A'$ && $A' \le B'$
BCA	$A' \le C'$ && $C' < B'$
CAB	$B' < A'$ && $A' \le C'$
CBA	$A' \le B'$ && $B' \le C'$

Largest projection exits *last*	
EOS	Logical statement
ABC	$C' > B'$ && $B' > A'$
ACB	$B' \ge C'$ && $C' > A'$
BAC	$C' > A'$ && $A' \ge B$
BCA	$A' \ge C'$ && $C' > B'$
CAB	$B' > A'$ && $A' \ge C'$
CBA	$A' \ge B'$ && $B' \ge C'$

As a conservative approach, the rightmost, or worst case, solution from the ranking above is reported from overlapping EOSs. As shown in Table 1, appropriate selection of inequality signs, either < > or ≤ ≥, outputs the worst-case EOS from coincident projections.

To illustrate the scheme, consider a tool with geometry α = 0° and γ = 90°. Under these circumstances, B' = C' at all points along the edge of the workpiece, as depicted in Figure 7. In the arrangement shown in the same figure, A is the *last* point to exit; however, since *B' = C'*, exit orders CBA and BCA overlap. The inequalities in Table 1 return CBA, the most burr-prone condition according to EOS theory.

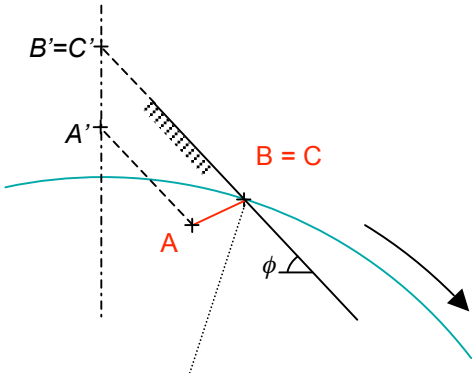

FIGURE 7. EXAMPLE OF OVERLAPPING EOS CONDITIONS CBA AND BCA.

EOS simulation example

Under most cutting conditions, EOS changes from less burr-prone to more burr-prone as radial tool engagement increases (Hashimura, 1994). Figures 8(a) and 8(b) show EOS simulations on the contours of an automotive transmission housing manufactured by DaimlerChrysler AG. The tool has double-positive rakes angles of 4˚ and a lead angle of 86˚. The cutter travels under forward rotation, counter-clockwise along a circular path with no offset with respect to the outer contour of the housing (a) and with an offset (b). In case (a), the outer contour of the workpiece is at lower radial tool engagement than the same contour in case (b). Therefore, toolpath (a) results in a more favorable EOS (BAC) and lower predicted burr formation along the outer contour than toolpath (b) (CBA). In both cases, the inner contour of the housing sees tool entry.

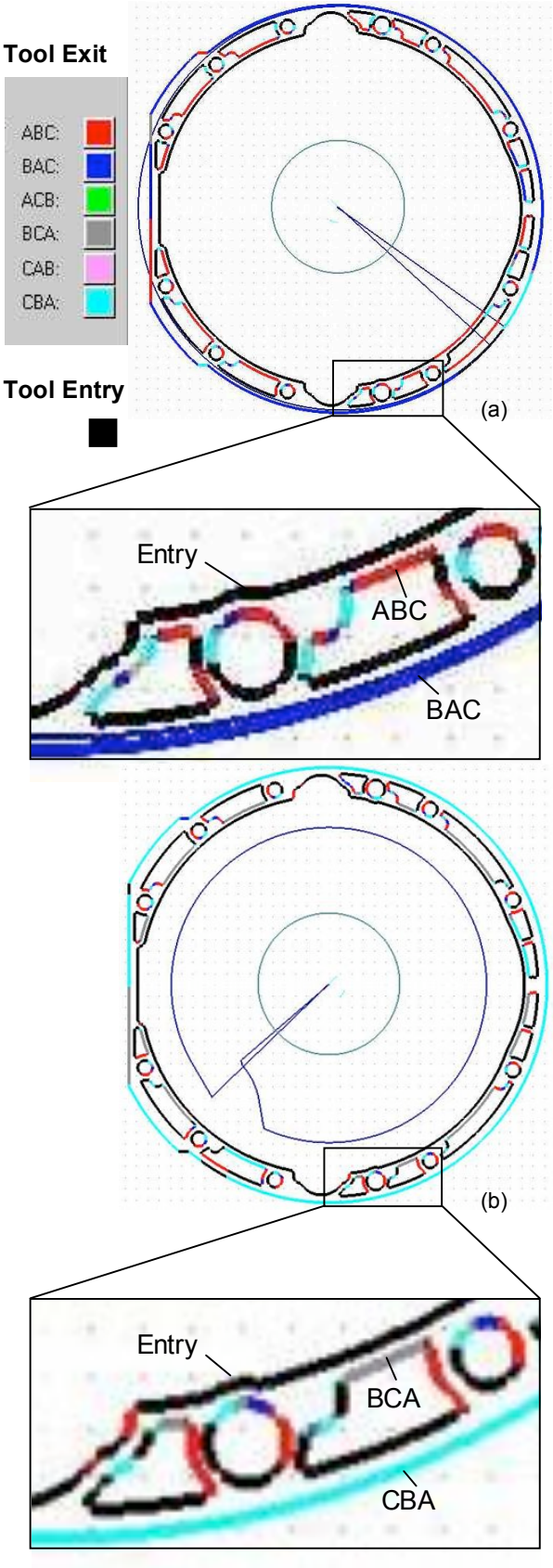

FIGURE 8. EOS SIMULATIONS. PATH (a) MINIMIZES UNFAVORABLE CBA REGIONS.

LIMITATIONS

The EOS algorithm presented is accurate under the assumption that the length of every segment P_1P_2 of the tessellated workpiece contour is equal or greater than *w*. In other words, it is presumed that the features of the workpiece are no smaller than the uncut chip thickness. This condition is met by the majority of parts in the automotive industry, where $w < 0.2$ mm under most finishing operations.

The exit order of point C, given by equations 3, 10, and 11, is valid for orthogonal relationship between the machined and exit surfaces (i.e. workpiece angle = 90°). A deviation from orthogonality will either retard or advance the exit time of C (t_c). Although a shift in t_c caused by a change in the workpiece angle could be easily incorporated into the equations, it is of no practical use. All other cutting parameters remaining constant (including EOS as calculated above), acute workpiece angles will always increase burr formation, whereas obtuse angles will always minimize plastic deformation leading to burr formation due to the added amount of backup material (e.g. Park and Dornfeld, 2000).

CONCLUSIONS

An algorithm for the simulation of exit order sequence (EOS), based on a Cartesian frame of reference and implemented in C++, has been developed and tested on automotive workpieces. Future work focuses on the integration of in-plane exit/entrance angle calculations to augment the burr prediction capabilities of the kinematic models.

ACKNOWLEDGEMENT

This research was funded by the Consortium on Deburring and Edge Finishing (CODEF) at the University of California, Berkeley. The invaluable support of Dipl.-Ing. Klaus Berger and Dipl.-Ing. Mischa Plickat, DaimlerChrysler AG Stuttgart – Untertürkheim, is gratefully acknowledged.

http://lma.berkeley.edu/CODEF/index.html

REFERENCES

Ávila, M., Dornfeld, D. (2004) "Burr Formation Mechanisms and Minimization Strategies at High Tool Engagement", *7th Int'l Deburring & Edge Finishing Conf.,* Berkeley, CA, June, pp. 191-200.

Bansal, A. (2002) Tool path planning in Face Milling for Burr Prevention, Masters Report, Dept. of Mechanical Engineering, UC Berkeley.

Chu, C-H, Dornfeld, D. (2000) "Tool Path Planning for Avoiding Exit Burrs", *J. Manufacturing Processes*, SME, Vol. 2, pp. 116-123.

Gillespie L, and Blotter, P. (1976) "The Formation and Properties of Machining Burrs" *Trans. ASME J. Engineering for Industry*, Ser. B 98, 2, pp. 66-74.

Hashimura, M., Hassamontr, J. (1995) "Effects of Radial Rake Angle and In-Plane Exit Angle in Burr Formation in Milling" 1994/95 *LMA Reports*, pp. 23-26.

Hashimura, M., Hassamontr, J., Dornfeld, D. (1999) "Effect of In-Plane Exit Angle and Rake Angles on Burr Height and Thickness in Face Milling Operation", *ASME J. of Manufacturing Sc. and Eng*., 121,13, pp. 13-19.

Ko, S. L., Dornfeld, D. (1996), "Burr Formation and Cutting in Oblique Cutting", *J. Materials Processing Technology*, 62, pp. 24-36.

Min, S., Dornfeld, D., Kim, J., Shyu, B. (2001), "Finite element modeling of burr formation in metal cutting," *Proc. 4th CIRP Int'l Workshop on Modeling of Machining Operations*, Delft, August, pp. 97-104.

Narayanaswami, R., Dornfeld. D. (1997), "Burr Minimization in Face Milling: A Geometric Approach", *ASME Trans.*, 170, pp. 170-177.

Park, I. (1995) "Modeling of Burr Formation Processes by FEM", 1994/95 *LMA Reports*, University of California, Berkeley, pp. 13-16.

Park, I, and Dornfeld, D (2000) "A Study of Burr Formation Processes Using the Finite Element Method Part II", *Trans. ASME J. Engineering Materials and Technology*, 122, pp. 229-237.

Shefelbine, W. (2004), "Influences on Burr Size During Face Milling of Aluminum Alloys and Cast Iron" *2003/04 LMA Reports*, University of California, Berkeley, pp. 76-81.